Ultrasonics 95 (2019) 6–12

Contents lists available at ScienceDirect

Ultrasonics

journal homepage: www.elsevier.com/locate/ultras

An experiment study on temperature characteristics of a linear ultrasonic motor using longitudinal transducers

He Li, Weishan Chen, Xinqi Tian, Junkao Liu*

State Key Laboratory of Robotics and System, Harbin Institute of Technology, Harbin 150001, Heilongjiang Province, China

ARTICLE INFO

Keywords:
Ultrasonic motor
Transducers
Temperature characteristics

ABSTRACT

The temperature characteristics of a T-shaped linear ultrasonic motor using longitudinal vibration transducers are reported. When the ultrasonic motor is excited by different voltages, the surface temperatures at the driving foot, PZT ceramic and end cap are tested by a thermal imager for obtaining the thermal characteristics of the motor under no-load condition. PZT ceramic shows the maximum temperature increase. Then, the variations of resonant frequencies, electromechanical coupling factors and mechanical Q-factors versus time, as well as the effect of the temperature on the resonance frequencies, electromechanical coupling factors and mechanical Q-factors, is measured and analysed under the long-term running. It is found that all the resonance frequencies and electromechanical coupling factors decrease as the increase of the temperature, as well as the mechanical Q-factors. In addition, the change of the output speed over temperature is tested and the obtained result shows the trend of decline. This work can provide useful guidelines for the design and optimization of linear ultrasonic motor operating in wide temperature range.

1. Introduction

Due to merits of compact structure, fast response, high power to weight ratio, self-locking in power failure, anti-disturbance of electromagnetism, ultrasonic motors (USMs) have gotten more and more attentions and been applied in many fields in recent years [1–5]. In previous studies, many scholars focus on the novel structure designs of USMs to improve some performance characteristics which target particular demands or broader range of applications [6–10]. However, the ambient environment temperature variation and temperature rise caused by energy loss in the electromechanical coupling process [11] will change the physical and material properties of the USMs. Furthermore, higher temperature can make lead zirconate titanate (PZT) materials which serve as the important part of the USMs suffer from the changes in materials properties such as dielectric permittivity [12], elastic coefficients [13], piezoelectric coefficients [14], hysteresis [15,16], even rapid aging and depolarization [17,18] resulting in the unstable operating and low life of the USMs eventually [19,20]. Therefore, effect of the temperature on the characteristics of the USMs cannot be ignored.

In recent studies, some researchers have carried out the study on the thermal characteristics of USMs. Traveling-wave rotatory ultrasonic motor (TWRUM), as a successful case applied in commercialization, has received attention in temperature dependence of motor performance [21–24]. In 2011, Lu et al. built the finite element model to analyse the temperature distributions on four TWRUMs with different size parameters [21]. Furthermore, in 2013, Lu et al. established a theoretical model to investigate the temperature-influenced output characteristics of the TWRUM based on FEM [22]. Li et al. proposed a model to evaluate the temperature rise of TWRUM considering the temperature-related varying dimension parameters [23]. Shokrollahi et al. investigated the heating effect of magnetic resonance imaging (MRI) system on the TWRUM used to drive surgical robot, it was found that the temperature increase can almost reach 10℃ in the motor which operated in the 3.0-Tesla MRI environment [24]. With respect to TWRUM, the temperature characteristics of standing wave ultrasonic motor (SWUM) were investigated by Li et al. based on the finite element analysis and finite difference method [25]. Chen et al. proposed a theoretical model based on finite element method and Coulomb's friction law for studying the effect of ambient temperature (−60 °C ~ 20 °C) on a piezoelectric actuated tracked mobile system [26]. However, the above theoretical and finite element methods for frictional interface are not compatible with stick-slip motion. Xu et al. presented a mechanical model for a longitudinal oscillation USM considering the sticking and slipping in the contact phase, and analysed the frequency-temperature characteristics of the stator [27]. Li et al. developed an

* Corresponding author.
E-mail address: junkaoliu@163.com (J. Liu).

https://doi.org/10.1016/j.ultras.2019.03.003
Received 6 December 2018; Received in revised form 22 January 2019; Accepted 1 March 2019
Available online 02 March 2019
0041-624X/ © 2019 Elsevier B.V. All rights reserved.

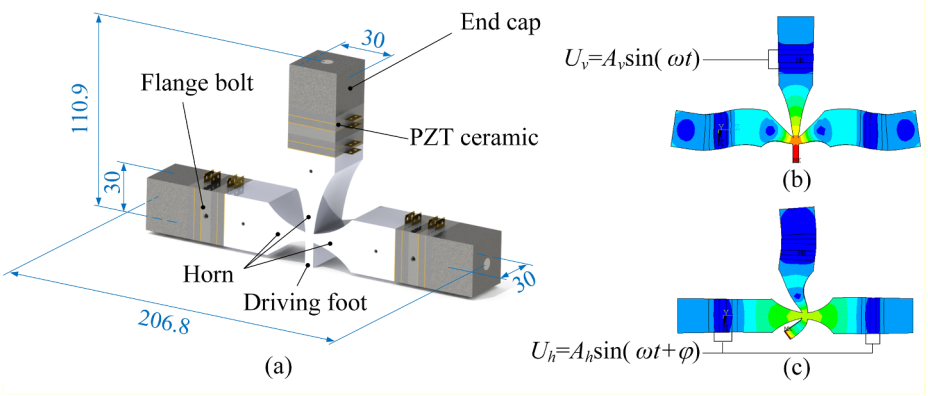

Fig. 1. Structure configuration and vibration modes of the motor: (a) Structure and dimensions (unit: mm), (b) Mode A, (c) Mode B [32].

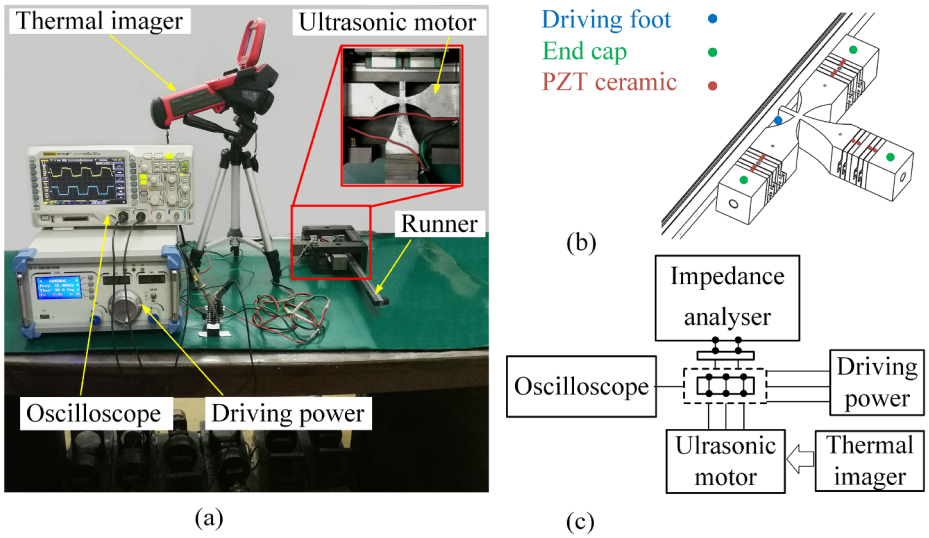

Fig. 2. The temperature measuring setup: (a) infrared test for the temperature rise on the motor, (b) the test point locations, (c) the schematic of the experiment setup for measuring impedance characteristic.

integrated dynamic model to research the thermal-mechanical-electric coupling dynamics in a bimodal USM [28], but the variant of electromechanical coupling factors with temperature was not predicted by this model. Furthermore, there is little research on the temperature characteristics of hybrid type USMs. Chen et al. proposed an piezoelectric actuator working in two orthogonal first bending modes which can keep operating at the high temperature (200 °C) [29]. The variations of resonance frequency, speed, load and efficiency with the increasing temperature are tested and analysed. Yang et al. analysed the mechanical output characteristics of a longitudinal hybrid type linear USM under different ambient temperature [30]. Liu et al. assessed five exciting methods for bending hybrid motors by investigating their thermal characteristics under no-load condition [31].

In this work, a high-power longitudinal-longitudinal hybrid type T-shaped ultrasonic motor [32] is taken as a study focus to obtain and analyse the temperature variations of different components under different driving voltages. The basic structure and the working principle of the T-shaped ultrasonic motor are given a brief description in Section 2. The experimental system is introduced in Section 3. The surface temperature variations of the different components of the motor with the time, the temperature dependence of the resonance frequencies, electromechanical coupling factors, mechanical Q-factors of transducers as well as the output speed of motor are discussed and analysed in Section 4, which is followed by a conclusion of Section 5.

2. Structure and working principle of T-shaped ultrasonic motor

In 2010, Liu et al. presented a high power longitudinal-longitudinal hybrid T-shaped ultrasonic motor, whose stator consisted of a vertical transducer and a horizontal transducer [32]. Fig. 1(a) shows the 3-D structure and dimensions of the stator. During the fabrication, the clamped stress of the PZT ceramics was set as 30 MPa, which was controlled by a torque wrench. The end cap is made of steel, the selected material of the horn is duralumin alloy, the PZT ceramic material is PZT-41, whose physical parameters are as follows:

$$[e]=\begin{bmatrix} 0 & 0 & -2.4 \\ 0 & 0 & -2.4 \\ 0 & 0 & 17.3 \\ 0 & 0 & 0 \\ 0 & 12.95 & 0 \\ 12.95 & 0 & 0 \end{bmatrix} \quad \mathrm{N/(V\cdot m)} \tag{1}$$

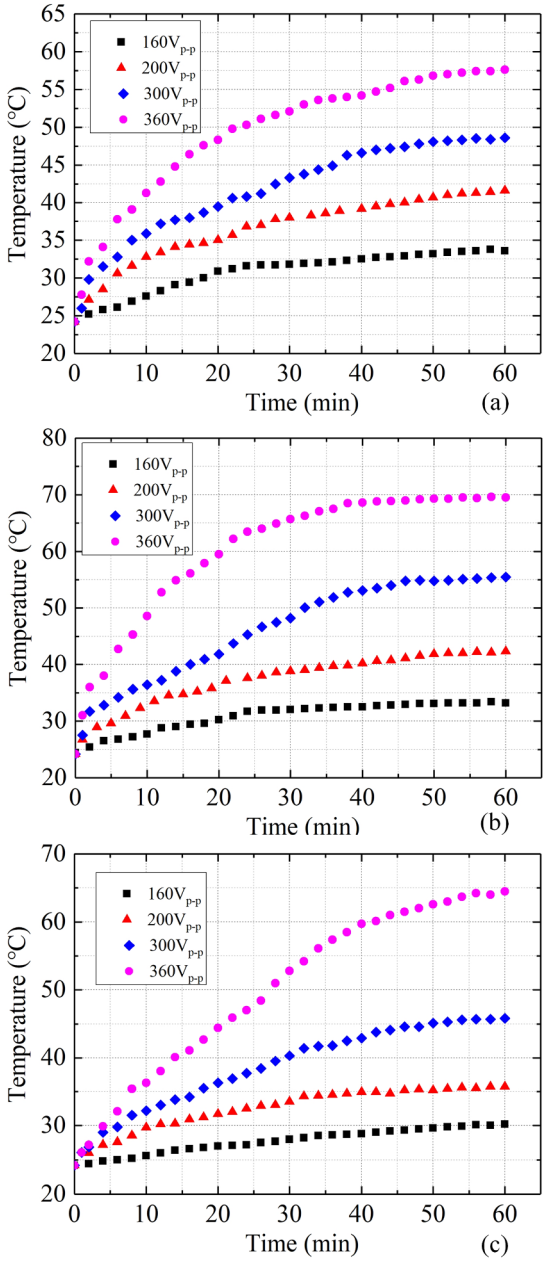

Fig. 3. Temperature changes of the driving foot, the PZT ceramic and the end cap of the motor under no load condition: (a) the driving foot, (b) the PZT ceramic, (c) the end cap.

$$[C^E] = \begin{bmatrix} 15 & 8.4 & 8.4 & 0 & 0 & 0 \\ 8.4 & 15 & 8.4 & 0 & 0 & 0 \\ 8.4 & 8.4 & 11.5 & 0 & 0 & 0 \\ 0 & 0 & 0 & 3.33 & 0 & 0 \\ 0 & 0 & 0 & 0 & 2.67 & 0 \\ 0 & 0 & 0 & 0 & 0 & 2.67 \end{bmatrix} \times 10^{10}\mathrm{N/m^2} \quad (2)$$

$$[\varepsilon^T] = \begin{bmatrix} 6.76 & 0 & 0 \\ 0 & 6.76 & 0 \\ 0 & 0 & 5.66 \end{bmatrix} \times 10^{-9}\mathrm{F}/m \quad (3)$$

where e, c^E, and ε^T denote the piezoelectric matrix, the stiffness matrix, and the dielectric matrix, respectively. As shown in Fig. 1(b) and (c), when two-phase alternating voltages U_v and U_h are applied on the vertical and horizontal transducers separately, mode A and mode B will be excited; these two modes can produce the vertical and horizontal displacements of the driving foot, respectively. If these two modes have equal resonant frequency and a temporal shift φ of 90°, an elliptical movement will be generated at the driving foot.

3. Experiments

Experimental research method is used to study the thermal characteristics of the T-shaped motor as the complexity of building a thermal-electrical-mechanical coupling mathematical model. As shown in Fig. 2, the experimental systems have been designed and established. In Fig. 2(a), a driving power is used to generate the two continuous square-wave signals with temporal shift of 90°, the working frequency is set as 25.35 kHz. The motor drives the runner to realize the reciprocating motion under the voltages of 160 V_{p-p}, 200 V_{p-p}, 300 V_{p-p} and 360 V_{p-p}, respectively. The waveforms of driving voltage signals are measured by an oscilloscope. A thermal imager (UTi 380, Uni-Trend, China) is used to measure the surface temperature of the motor including the driving foot, the PZT ceramic and the end cap, the test points are shown in Fig. 2(b). The temperatures of the T-shaped ultrasonic motor are tested considering the fictional coupling under no-load condition (the preload between the driving foot and the runner is set as 240 N). The motor works continuously for one hour. The output speed of the motor is measured by a magnetic sensor (MSK200/1, SIKO, Germany). Furthermore, an impedance analyser (Agilent 4294A, Agilent Technologies, USA) is used to test the impedance of the two transducers to calculate the resonance frequencies, electromechanical coupling factors and mechanical Q-factors, as shown in Fig. 2(c).

4. Results and discussions

4.1. Temperature characteristics of T-shaped USM

As the changes of the surface temperatures in the vertical and horizontal transducers are nearly the same, Fig. 3 only shows the temperature variations of the driving foot, the PZT ceramic and the end cap in the vertical transducer under different driving voltages.

The temperature at the driving foot rises from 24.2 °C to 33.1 °C under the voltage of 160 V_{p-p} and keeps relatively stable 25 min later, as shown in Fig. 3(a); when the driving voltage is larger than 200 V_{p-p}, the temperature rises faster and remains rising slowly about 25 min later. The temperature increases with the rise of driving voltages and shows a rise of 8.9 °C, 17.4 °C, 24.4 °C, 33.4 °C in one hour under the above driving voltages, respectively. One of the main causes of temperature rise is the dielectric and mechanical damping loss of electromechanical coupling [28], and the other reason is the friction coupling between the driving foot and the runner. In addition, as the motor runs continuously for one hour, the wear behavior at contact interface between the stator and runner will make the temperature rise more complex.

The average value of temperatures at the four PZT ceramics were calculated, and its variation versus time is shown in Fig. 3(b), the temperature increases from 24.2 °C to 33.4 °C with a rise of 9.2 °C under the driving voltage of 160 V_{p-p}, which is a little higher than the temperature increase of the driving foot. Under the driving voltage of 200 V_{p-p}, the temperature at PZT ceramic keeps slow increasing after about 25 min, and rises by 18.2 °C, which is similar to the temperature rise of the driving foot. Furthermore, the temperature at the PZT ceramic shows a slow increasing at 300 V_{p-p} and 360 V_{p-p} about 40 min later, and the PZT ceramic is subjected to higher temperature than driving foot after the motor stops running. Due to the close proximity of the PZT ceramic and the electrode, the temperature of the PZT ceramic rises higher than that of the driving foot, particularly at high driving voltages. The maximum temperature can reach 69.5 °C with an increase of

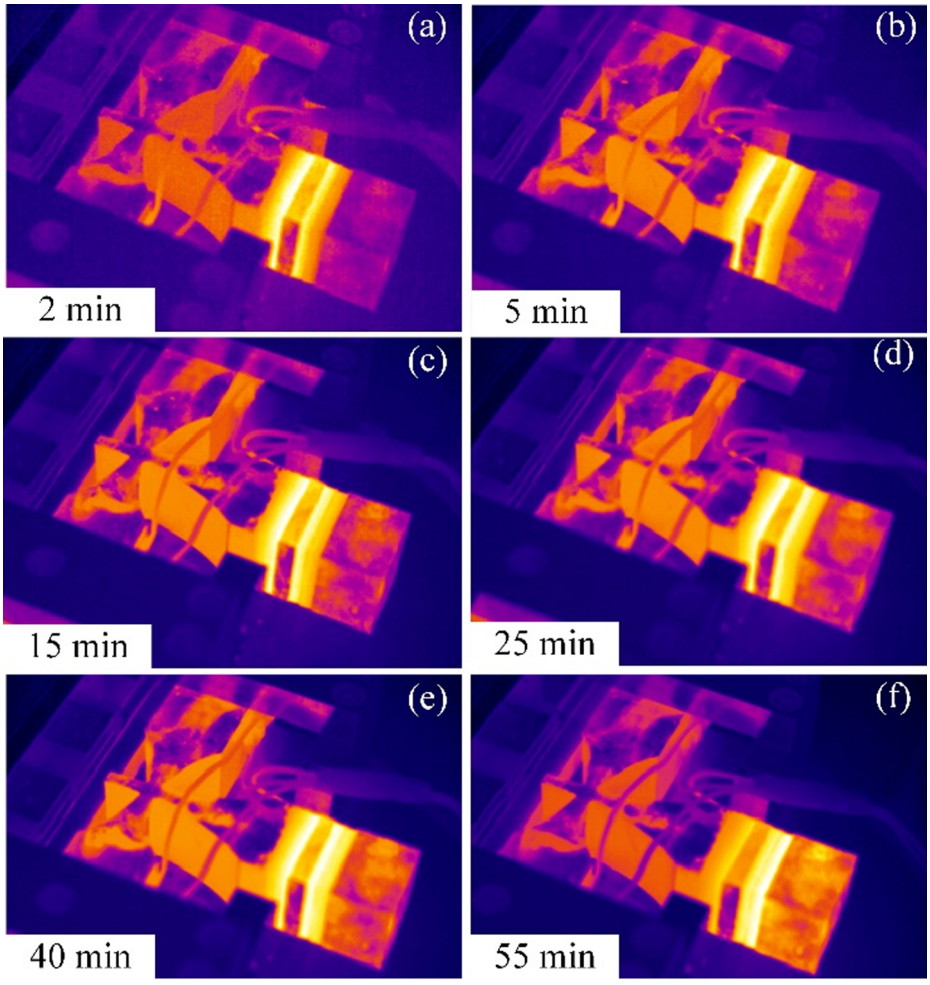

Fig. 4. Thermal imaging picture of the motor under the voltage of 360 $V_{p\text{-}p}$.

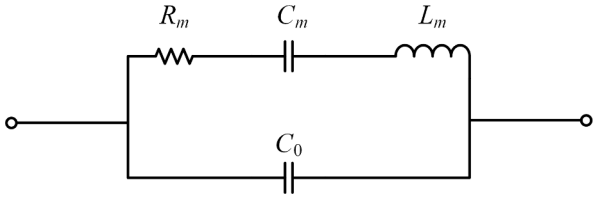

Fig. 5. Equivalent circuit model of the piezoelectric transducer.

45.3 °C under the voltage of 360 $V_{p\text{-}p}$ one hour later.

As can be seen in Fig. 3(c), although the temperature variation tendency of the end cap is similar to that of the driving foot. Heat conduction from the electrodes accounts for a major factor in temperature rise, and there is no frictional coupling. As the heat transfer will take some time, so the temperature at the end cap still keeps slow upward trend. The temperature rises up to 30.1 °C with an increase of 5.9 °C under the voltage of 160 $V_{p\text{-}p}$ within one hour, and the temperature increases by 11.5 °C and 21.6 °C when the motor is excited by the voltages of 200 $V_{p\text{-}p}$ and 300 $V_{p\text{-}p}$ respectively, which shows the lower temperature variations than driving foot. The difference is a temperature increase of 40.3 °C under the voltage of 360 $V_{p\text{-}p}$, which may be caused by the more heat transfer from the PZT ceramic to end cap under high driving voltage.

In order to observe the heat variations tendency of motor clearly, the surface temperature distribution versus time under the voltage of 360 $V_{p\text{-}p}$ is shown in Fig. 4. The PZT ceramic keeps the high-temperature relative to the end cap and driving foot after the motor works. The end cap shows the obvious temperature changes over time, just as the Fig. 3(c) shows.

With the aid of an impedance analyser, the resonance frequencies of two transducers can be measured and the electromechanical coupling factors and mechanical Q-factors also can be calculated based on the equivalent circuit model, as shown in Fig. 5 [33].

The electromechanical coupling factor k and Q-factors Q_m are described as follows:

$$k = \sqrt{\frac{C_m}{C_0 + C_m}} \tag{4}$$

$$Q_m = \frac{1}{R_m}\sqrt{\frac{L_m}{C_m}} \tag{5}$$

where C_0 is the static capacitance, R_m, L_m and C_m are the equivalent resistance, inductance and capacitance, respectively. Under the voltage of 360 $V_{p\text{-}p}$, the motor runs for one hour continuously and then naturally cools down again about one hour. According to the Fig. 6, we can see the changes of the resonance frequencies (f_v and f_h), electromechanical coupling factors (k_v and k_h) and mechanical Q-factors (Q_{m_v} and Q_{m_h}) of the vertical and horizontal transducers where the subscript v and h of the f_v and f_h (k_v and k_h, Q_{m_v} and Q_{m_h}) represent the vertical transducer and horizontal transducer, respectively.

According to the Fig. 6(a), it is observed that the resonance

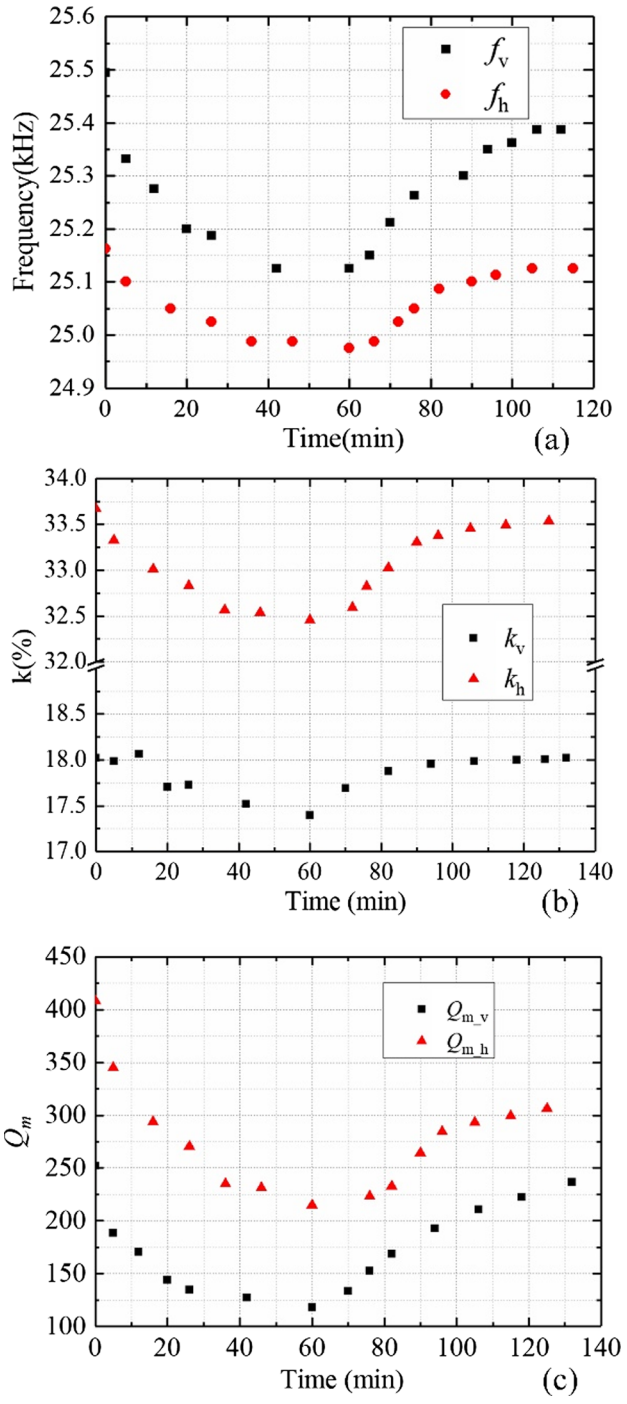

Fig. 6. Resonance frequencies, electromechanical coupling factors and mechanical Q-factor of two transducers versus time: (a) the resonance frequencies, (b) the electromechanical coupling factors, (c) the mechanical Q-factors.

frequencies of two transducers decrease by 1.45% and 0.75% nonlinearly within the first one hour respectively, and then recovers gradually after the motor stop running. Fig. 6(b) shows the changing trend of the electro-mechanical coupling factors over time is similar to the resonance frequencies, the difference is that the electromechanical coupling factor of the horizontal transducer is higher than that of the vertical transducer, and has a drop of 3.6% after the motor runs for one hour relative to the slight drop of 3.47% in the vertical transducer. The curves of mechanical Q-factors with temperature changes are shown in Fig. 6(c), there is a higher mechanical Q-factor in horizontal transducer than that in vertical transducer all the time, and the Q-factors of horizontal and vertical transducers decline by 46.4% (from 408.3 to 214.7) and 53.2% (from 252 to 134) within one hour. The above three mechanical characteristics of the motor gradually recover the initial level after the motor stops working. In fact, the Curie temperature (T_C) of PZT-4 is between 300 °C and 400 °C and the PZT ceramic materials will suffer from depolarization above the temperature T_C. According to Figs. 3 and 6, the maximum operating temperature of the PZT ceramic material is no more than 70 °C which is much lower than the temperature T_C under the voltage of 360 $V_{p\text{-}p}$, and mechanical performance of the motor can return to normal operation after the driving voltage is turned off.

Fig. 7 indicates the effect of temperature on the resonance frequencies using the PZT ceramic as reference object. The relationships between resonance frequencies of two transducers and temperature are obtained by linear fitting, as follows:

$$f_v(T) = 25676.582 - 8.529T \tag{6}$$

$$f_h(T) = 25286.38 - 5.5T \tag{7}$$

It is found that the resonance frequencies of two transducers decrease linearly with the increase of the temperature, this is mainly due to the effect of temperature on the properties of the material, such as elastic coefficient [13,34], coefficient of thermal expansion [35] and thermal stress [36]. The above test results show that the temperature has a remarkable effect on characteristic of USM, which affects the continuous and stable running of USM. Therefore, during the design process, a dynamic model or FEM of the USM should be constructed to decline the influence of temperature factors such as resonance frequencies. In addition, considering the temperature characteristic of materials, the optimization methods of structure and materials process are also considered to minimum their impacts [37].

Fig. 8 shows the electro-mechanical coupling factors and the variations of mechanical Q-factors of two transducers with temperature. In Fig. 8(a), the electromechanical coupling factors decrease gradually as the increasing of temperature. Similarly, as can be seen in Fig. 8(b), both the mechanical Q-factors of two transducers also decline with the temperature increasing nonlinearly, and are different from the linear change trends of resonance frequencies. The degradation of the mechanical Q-factor with increasing temperature which indicates that the temperature rise of the motor will result in larger mechanical loss of two transducers and the degradation of mechanical performance of the motor.

In order to observe the output speed change caused by temperature rise of each component of the motor, the speed-temperature curves of the motor excited by the voltage of 360 $V_{p\text{-}p}$ under no-load condition are shown in Fig. 9 (the working frequency is set as 25.35 kHz). At the start, the temperatures at different components of the motor are same and the maximum output speed is 719.35 mm/s, but the speed decreases gradually with the rises of temperatures at different components, and has a drop of 51% at last. The temperature variation of each component of the motor has an obvious impact on the output speed, and shows the similar varying tendency of speed. It can be explained that the working frequency deviates from the resonance frequencies as the temperatures at different parts of the motor change together, resulting in the decreases of the amplitude and vibration velocity of the driving foot. This effect ultimately leads to the decline of the output speed as that the speed is proportional to the vibration velocity: the microscopical vibration of the driving foot is transmitted to the macroscopic linear motion of the runner by the friction between the driving foot and runner. Therefore, due to the mechanical output performance

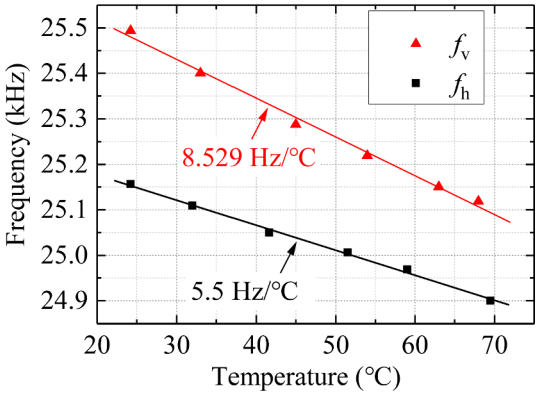

Fig. 7. Temperature dependence of resonance frequencies of two transducers.

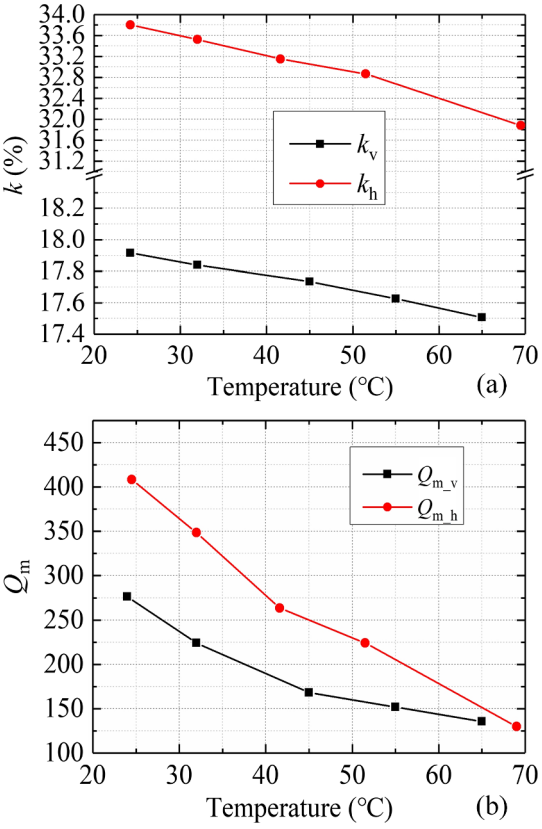

Fig. 8. The electromechanical coupling factors and the mechanical Q-factor of two transducers versus the temperature of the PZT ceramic: (a) the vertical transducer, (b) the horizontal transducer.

drop caused by the temperature increasing of the motor, it is essential to take some temperature control or compensation measures for the continuous and stable working of the motor [20,38].

4.2. Temperature characteristics of other hybrid type USMs

For other hybrid type USMs with the similar working principle relative to the T-shaped USM, it can be predicted that the temperature will increase rapidly at first and then tend to be stable when the USM works continuously due to the energy loss, but the time to reach stable temperature is different as the discrepancies of structural shapes and parameters between different hybrid type USMs. Simultaneously, the mechanical loss increases with the working of the USM as the

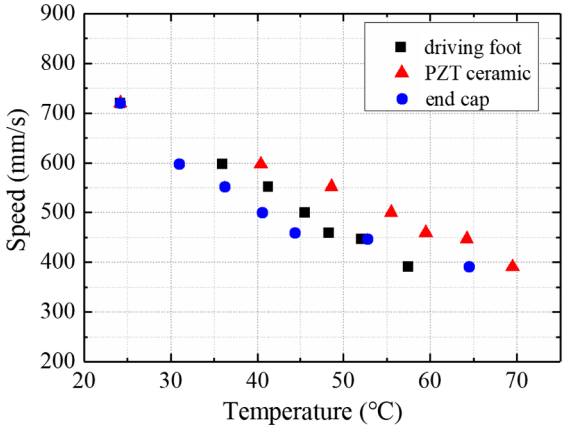

Fig. 9. Speed versus temperature under the voltage of 360 $V_{p\text{-}p}$.

continuous energy loss, so the mechanical Q-factors will present decline trend. The variations of the electro-mechanical coupling factors with temperature will perform slight drop or fluctuation. In addition, the material properties of metal and piezoelectric materials vary with the temperature, such as the elastic coefficient, so the resonance frequencies of USMs will decline with continuous working, which can cause the decrease of the output speed.

5. Conclusion

This study mainly analyses the influence of temperature on the T-shaped ultrasonic motor. The temperature changes of different components under no-load condition are tested by applying different driving voltages. The maximum temperature at the PZT ceramic can reach 69.5 °C with an increase of 45.3 °C. As the driving voltage increases, the temperature becomes higher. The resonance frequencies, electromechanical coupling factors and mechanical Q-factors decrease with the increasing of temperature, and they will return to original level when the motor stops running and cools down, which means the whole changing process is reversible and the PZT materials has not suffered from depolarizing. In addition, the variations of resonance frequencies with the temperature are approximately linear. The influence of temperature on the output speed is also studied. The output speed will experience a decline of 51% after continuous working of one hour. Furthermore, the temperature characteristics of other type USMs using the hybrid of vibration modes may have the similar changing trend.

Acknowledgments

This work was supported in part by the National Natural Science Foundation of China (No. 51622502), in part by the Foundation for the Author of National Excellent Doctoral Dissertation of China (No. 201428), in part by the Foundation for Innovative Research Groups of the National Natural Science Foundation of China (Grant No. 51521003) and in part by the Fok Ying Tung Education Foundation (No. 151053).

References

[1] T. Hemsel, J. Wallaschek, Survey of the present state of the art of piezoelectric linear motors, Ultrasonics 38 (2000) 37–40.
[2] Y.L. Shi, C.S. Zhao, W.Q. Huang, Linear ultrasonic motor with wheel-shaped stator, Sens. Actuator A-Phys. 161 (2010) 205–209.
[3] D.M. Xu, Y.X. Liu, S.J. Shi, J.K. Liu, W.S. Chen, L. Wang, Development of a non-resonant piezoelectric motor with nanometer resolution driving ability, IEEE-ASME Trans. Mechatron. 23 (2018) 444–451.
[4] S. Sherrit, Smart material/actuator needs in extreme environments in space, in: Proc. of the SPIE Smart Structure Conference San Diego, USA, 2005, pp. 335–346.

[5] Y.X. Liu, L. Wang, Z.Z. Gu, Q.Q. Quan, J. Deng, Development of a two-dimensional linear piezoelectric stepping platform using longitudinal-bending hybrid actuators, IEEE Trans. Ind. Electron. 66 (2019) 3030–3040.
[6] A. Kanada, T. Mashimo, K. Terashima, Flexible ultrasonic motor using an output coil spring slider, Proc. of the IEEE/RSJ International Conference on Intelligent Robots and Systems (IROS) Canada, 2017, pp. 5616–5621.
[7] S.J. Zhang, J.K. Liu, J. Deng, Y.X. Liu, Development of a novel two-DOF pointing mechanism using a bending-bending hybrid piezoelectric actuator, IEEE Trans. Ind. Electron. (2018), https://doi.org/10.1109/TIE.2018.2883255.
[8] J.K. Liu, Y.X. Liu, L.L. Zhao, D.M. Xu, W.S. Chen, J. Deng, Design and experiments of a single-foot linear piezoelectric actuator operated in stepping mode, IEEE Trans. Ind. Electron. 65 (2018) 8063–8071.
[9] P.H. Goh, M.-J. Li, N.-T. Tsou, The design and analysis for low-frequency piezoelectric cymbal transducers, Ceram. Int. 43 (2017) S49–S54.
[10] Y.X. Liu, J.P. Yan, L. Wang, W.S. Chen, A two-DOF ultrasonic motor using a longitudinal-bending hybrid sandwich transducer, IEEE Trans. Ind. Electron. 66 (2019) 3041–3050.
[11] J.h. Hu, S.-F. Ho, E.-L. Ong, J.L. Du, An experimental investigation of the temperature field in small piezoelectric vibrators, Ultrasonics 41 (2004) 731–735.
[12] A.V. Mezheritsky, Elastic, dielectric, and piezoelectric losses in piezoceramics: How it works all together, IEEE Trans. Ultrason. Ferroelectr. 51 (2004) 695–707.
[13] Z. Gubinyi, C. Batur, A. Sayir, F. Dynys, Electrical properties of PZT piezoelectric ceramic at high temperatures, J. Electroceram. 20 (2007) 95–105.
[14] K. Nagata, E. Harashima, Improvement of temperature-dependence of piezoelectric elements, Jpn. J. Appl. Phys. 1 (33) (1994) 5348–5351.
[15] D. Habineza, M. Zouari, M. Hammouche, Y. Le Gorrec, M. Rakotondrabe, Characterization and modeling of the temperature effect on the piezoelectric tube actuator, in: Proc. of the 7th IFAC Symposium on Mechatronic Systems (MECHATRONICS), 2016, pp. 354–360.
[16] J. Zou, G.Y. Gu, High-precision tracking control of a soft dielectric elastomer actuator with inverse viscoelastic hysteresis compensation, IEEE-ASME Trans. Mechatron. (2018), https://doi.org/10.1109/TMECH.2018.2873620.
[17] T. Stevenson, D.G. Martin, P.I. Cowin, A. Blumfield, A.J. Bell, T.P. Comyn, P.M. Weaver, Piezoelectric materials for high temperature transducers and actuators, J. Mater. Sci.-Mater. Electron. 26 (2015) 9256–9267.
[18] J. Pritchard, R. Ramesh, C.R. Bowen, Time–temperature profiles of multi-layer actuators, Sens. Actuator A-Phys. 115 (2004) 140–145.
[19] L. Petit, N. Rizet, R. Briot, P. Gonnard, Frequency behaviour and speed control of piezomotors, Sens. Actuator A-Phys. 80 (2000) 45–52.
[20] M.A. Tavallaei, S.F. Atashzar, M. Drangova, Robust motion control of ultrasonic motors under temperature disturbance, IEEE Trans. Ind. Electron. 63 (2016) 2360–2368.
[21] X.L. Lu, J.H. Hu, C.S. Zhao, Analyses of the temperature field of traveling-wave rotary ultrasonic motors, IEEE Trans. Ultrason. Ferroelectr. Freq. Control. 58 (2011) 2708–2719.
[22] X.L. Lu, S.Q. Zhou, C.S. Zhao, Finite element method analyses of ambient temperature effects on characteristics of piezoelectric motors, J. Intell. Mater. Syst. Struct. 25 (2013) 364–377.
[23] S. Li, W. Ou, M. Yang, C. Guo, C. Lu, J. Hu, Temperature evaluation of traveling-wave ultrasonic motor considering interaction between temperature rise and motor parameters, Ultrasonics 57 (2015) 159–166.
[24] P. Shokrollahi, J. Drake, A. Goldenberg, Measuring the temperature increase of an ultrasonic motor in a 3-tesla magnetic resonance imaging system, Actuators 6 (2017) 20.
[25] S.Y. Li, M. Yang, Analysis of the temperature field distribution for piezoelectric plate-type ultrasonic motor, Sens. Actuator A-Phys. 164 (2010) 107–115.
[26] D. Chen, L. Wang, J. Liu, J. M. Jin, Analysis on ambient temperature effects on piezoelectric actuated tracked mobile system, in: Proc. of the 2016 Symposium on Piezoelectricity, Acoustic Waves, and Device Applications, 2016, pp. 140–144.
[27] X. Xu, Y.C. Liang, H.P. Lee, W.Z. Lin, S.P. Lim, K.H. Lee, X.H. Shi, Mechanical modeling of longitudinal oscillation ultrasonic motors and temperature effect analysis, Smart Mater. Struct. 12 (2003) 514–523.
[28] X. Li, Z.Y. Yao, Y.G. He, S.C. Dai, Modeling and experimental investigation of thermal-mechanical-electric coupling dynamics in a standing wave ultrasonic motor, Smart Mater. Struct. 26 (2017) 095044.
[29] J. Chen, Z. Chen, X. Li, S. Dong, A high-temperature piezoelectric linear actuator operating in two orthogonal first bending modes, Appl. Phys. Lett. 102 (2013) 052902.
[30] L. Yang, C. Jiang, Z.Y. Yao, The research on the performance of linear ultrasonic motor under different temperature, J. Vibroeng. 16 (2014) 792–799.
[31] Y.X. Liu, S.J. Shi, D.W. Wang, W.S. Chen, D.M. Xu, Research on the thermal characteristics of bending hybrid piezoelectric actuators under different exciting methods, Ceram. Int. 43 (2017) S15–S20.
[32] Y.X. Liu, W.S. Chen, J.K. Liu, S.J. Shi, A high-power linear ultrasonic motor using longitudinal vibration transducers with single foot, IEEE Trans. Ultrason. Ferroelectr. 57 (2010) 1860–1867.
[33] J.S. Kim, K. Choi, I. Yu, A new method of determining the equivalent circuit parameters of piezoelectric resonators and analysis of the piezoelectric loading effect, IEEE Trans. Ultrason. Ferroelectr. Freq. Control. 40 (1993) 424–426.
[34] T. Kamiya, R. Mishima, T. Tsurumi, M. Daimon, T. Nishimura, Mechanism of temperature-dependence of piezoelectric properties for Pb(Zr, Ti)O3, Jpn. J. Appl. Phys. 32 (1993) 4223–4226.
[35] C.W. Bert, V. Birman, Effects of stress and electric field on the coefficients of piezoelectric materials: One-dimensional formulation, Mech. Res. Commun. 25 (1998) 165–169.
[36] P.M. Weaver, T. Stevenson, T. Quast, G. Bartl, T. Schmitz-Kempen, P. Woolliams, A. Blumfield, M. Stewart, M.G. Cain, High temperature measurement and characterisation of piezoelectric properties, J. Mater. Sci.-Mater. Electron. 26 (2015) 9268–9278.
[37] Y. Nambu, T. Takashima, A. Inagaki, Robust design method and thermostatic experiment for multiple piezoelectric vibration absorber system, Smart Mater. Struct. 24 (2015) 125016.
[38] Y. Yano, K. Iida, T. Sakabe, K. Yabugami, Y. Nakata, Approach to speed control using temperature characteristics of ultrasonic motor, in: Proc. of the 47th Midwest Symposium on Circuits and Systems, 2004, pp. 155–158.